Inorganic Chemistry

Article

pubs.acs.org/IC

Macrocyclization of the ATCUN Motif Controls Metal Binding and Catalysis

Kosh P. Neupane, Amanda R. Aldous, and Joshua A. Kritzer*

Department of Chemistry, Tufts University, 62 Talbot Avenue, Medford, Massachusetts 02155, United States

Supporting Information

ABSTRACT: We report the design, synthesis, and characterization of macrocyclic analogues of the amino-terminal copper and nickel binding (ATCUN) motif. These macrocycles have altered pH transitions for metal binding, and unlike linear ATCUN motifs, the optimal cyclic peptide **1** binds Cu(II) selectively over Ni(II) at physiological pH. UV−vis and EPR spectroscopy showed that cyclic peptide **1** can coordinate Cu(II) or Ni(II) in a square planar geometry. Metal binding titration and ESI-MS data revealed a 1:1 binding stoichiometry. Macrocyclization allows for coordination of Cu(II) or Ni(II) as in linear ATCUN motifs, but with enhanced DNA cleavage by the Cu(II)-**1** complex relative to linear analogues. The Cu(II)-**1** complex was also capable of producing diffusible hydroxyl radicals, which is unique among ATCUN motifs and most other common copper(II) chelators.

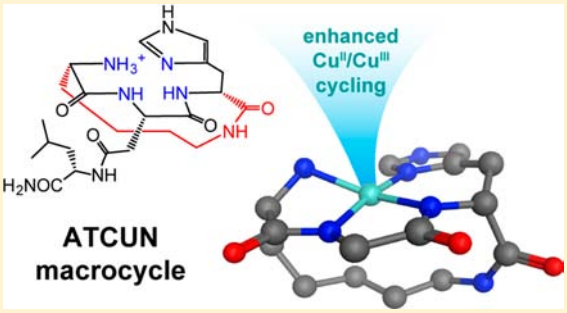

INTRODUCTION

Peptide backbones offer a modular, chiral, and synthetically accessible platform for exploring conformational effects on metal binding.[1,2] Diverse peptides and proteins use histidyl residues for the coordination of metal ions including Cu(II) and Ni(II).[2−5] The precise positioning of histidine imidazole groups plays a significant role in the coordination chemistry of the overall polypeptide.[3,6] His-mediated coordination of Cu(II) and Ni(II) results in high thermodynamic stability of the metal complex, which is often further reinforced by metal ion-induced deprotonation of adjacent backbone amides.[5] This is exemplified by the amino-terminal copper and nickel (ATCUN) motif, originally identified in serum albumin proteins, which consists of the tripeptide with free N-terminus NH_2-Xaa-Xaa-His (where Xaa is any amino acid; Figure 1). ATCUN motifs bind Cu(II) or Ni(II) in a square planar geometry using the N-terminal amine, the imidazole, and two amide nitrogens. Decades of investigations into the ATCUN motif have yielded a detailed structural and mechanistic picture of how these peptides bind Cu(II) and Ni(II), and how the ligand modulates the redox properties of the metal ion.[7−9] The ATCUN motif has been used as a catalyst for selective DNA and protein cleavage,[7−17] protein−protein cross-linking,[18] enzyme inhibition,[19] and damaging malignant cells.[20]

Early experiments by Margerum and others demonstrated that macrocyclization can profoundly alter the thermodynamics and kinetics of metal binding for nonpeptidic and peptidic ligands.[1,21−23] The powerful effects of ligand macrocyclization on metal-binding behavior have been exploited for the design of metallopeptide complexes suitable for selective metal ion recognition, ion transport, metalloenzyme modeling, and catalysis.[24−26] Macrocyclic ligands have also been widely used in biomedical applications as MRI contrast agents,[27,28] luminescence probes,[29,30] carriers for drug delivery,[31] and catalysts for selective nucleic acid cleavage.[32]

Herein we report macrocyclic analogues of the ATCUN motif that show uniquely enhanced redox properties. Previously, ATCUN variants were cyclized via amide formation with the N-terminus, which resulted in large decreases in binding affinity and disruption of the characteristic square planar complex. For example, Brasun and co-workers synthesized and characterized a series of cyclic tetrapeptides of the form cyclo-(His-Xaa-His-Xaa), where Xaa represents various amino acids, and found a variety of coordination environments for Cu(II) (N, 2N, 3N, and 4N equatorial donor sets) due to the stepwise deprotonation of amides from the peptide backbone.[33,34] In other work, six mononuclear Cu(II)-peptide complexes of cyclo-(HGHK) were observed at pHs ranging from 3 to 11. These cyclic peptides bound Cu(II) with substantially lower affinity than linear ATCUN motifs.[34]

We hypothesized that application of a macrocyclic constraint that did not alter the N-terminal amine would permit more careful design of square planar complexes with tunable selectivity and redox activity. We used the known crystal structure of Cu(II)-bound Gly-Gly-His-$CONH_2$ to model various macrocyclic constraints, while maintaining the square planar coordination geometry (Figure 1a).[35] On the basis of this exercise, we predicted that cyclic peptide **1** would be able to bind Cu(II) or Ni(II) in a similar square planar geometry. Compounds **2** and **3**, diastereomers of **1**, were predicted to be

Received: December 21, 2012
Published: February 19, 2013

   dx.doi.org/10.1021/ic302820z | Inorg. Chem. 2013, 52, 2729−2735

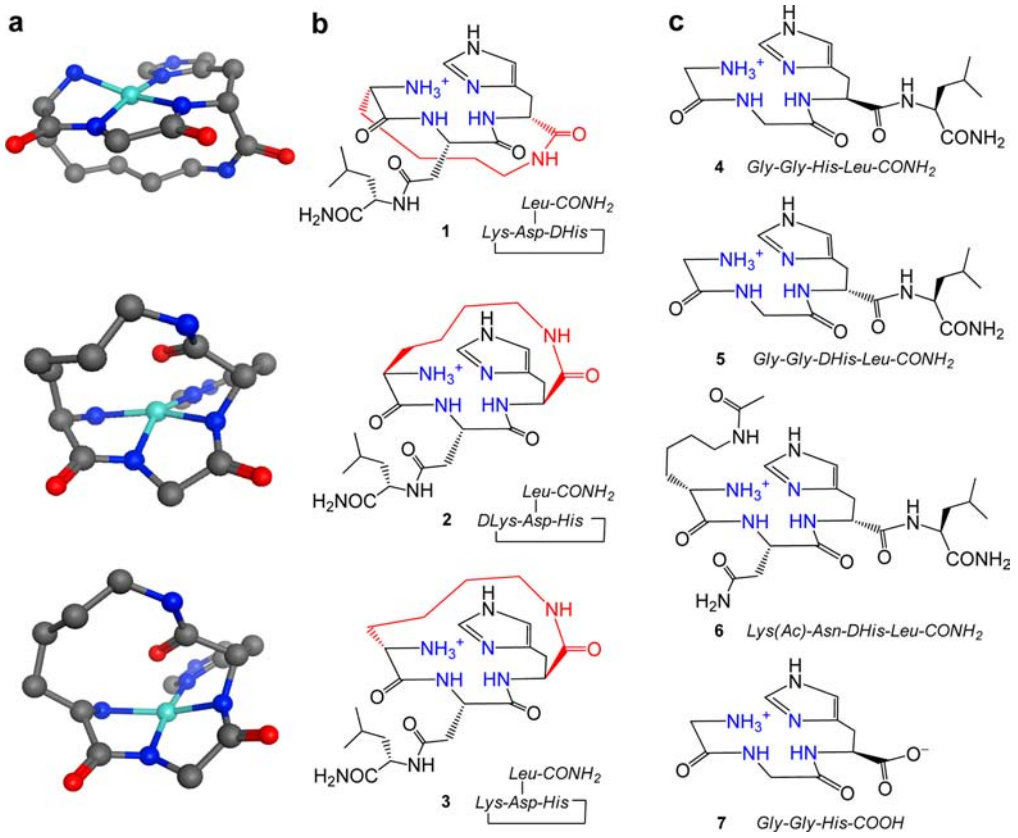

Figure 1. ATCUN-containing linear and cyclic peptides. (a) Models of peptide macrocycles **1**−**3** bound to Cu(II) demonstrating predicted strain between peptide conformation and square planar coordination geometry. Carbons are shown in gray, nitrogens in blue, oxygens in red, and copper in cyan. Leu residues and side chains of Asp/Asn residues are omitted for clarity. (b) Chemical structures of cyclic peptides **1**−**3** at pH = 7.5. Nitrogens critical for metal ion binding are shown in blue, and macrocycle linkers are shown in red. (c) Chemical structures of linear peptides **4**−**7** at pH = 7.5. Nitrogens critical for metal ion binding are shown in blue.

able to bind metal ions in a square planar geometry, but with substantial ring strain.

EXPERIMENTAL SECTION

Materials. Fmoc (*N*-α-(9-Fluorenyl methyloxycarbonyl)) protected amino acids, Rink Amide resin, *N*-hydroxybenzotriazole (HOBt), and 2-(1*H*-benzotriazole-1-yl)-1,1,3,3-tetramethyluronium hexafluorophosphate (HBTU) were purchased from either NovaBiochem or AnaSpec; diisopropylethylamine (DIPEA), acetic anhydride, pyridine, trifluoroacetic acid (TFA), triisopropyl silane (TIPS), and dimethyl formamide (DMF) were purchased from Sigma-Aldrich. Component amino acids included the following: Fmoc-Gly-OH, Fmoc-Asp-(OAll), Fmoc-Asn(Trt)-OH, Boc-Lys(Fmoc)-OH, Boc-DLys(Fmoc)-OH, Fmoc-Lys(Ac)-OH, and Fmoc-His(Trt)-OH, Fmoc-DHis(Trt)-OH, and Fmoc-Leu-OH. Palladium tetrakis-triphenylphosphine ($Pd(PPh_3)_4$) (Fisher), copper(II) chloride dihydrate (Sigma), nickel(II) chloride hexahydrate (Sigma-Aldrich), cobalt(II) chloride hexahydrate (Sigma-Aldrich), gold(III) chloride (Sigma-Aldrich), sodium tetrachloroplatinate(II) hydrate (Acros Organics), sodium tetrachloropalladate(II) trihydrate (Strem Chemicals), and all other chemicals were used as received without modification. All ultrapure water was deionized water that was further filtered using a Barnstead Ultrapure UF system to ensure resistivity was greater than 17.8 MΩ.

Peptide Modeling. Molecular Operating Environment (ChemComp) software was used to build models of macrocyclic ATCUN variants based on the crystal structure parameters for the ATCUN-Cu(II) complex.[35] Models were energy-minimized using the MMFF94x forcefield. While this forcefield is not well-defined for copper, the modeling exercises were useful for examining torsional strains within the macrocyclic scaffolds.

Peptide Synthesis and Purification. Leucine residues were added to the C-termini of linear peptides and to the aspartate side chain of cyclic peptides in order to promote retention on reverse-phase HPLC columns. Peptides **1** to **6** were synthesized manually using standard Fmoc solid-phase synthesis protocols. Rink Amide resin (0.20 mmol/g) was used and couplings were performed with HBTU/HOBt/DIPEA (5:5:10). For cyclic peptides, allyl-protected C-termini were deprotected using $Pd(PPh_3)_4$ prior to Fmoc deprotection and cyclized overnight using PyBOP/Cl-HOBt/DIEA (5:5:10 equivalents). All peptides were cleaved off the resin using TFA/TIPS/H_2O (95:3:2). The volume was reduced by rotary evaporation and peptides were ether-precipitated.[36] Peptides were purified using HPLC on a preparative-scale C8 column (solvent A was water/0.1% TFA, solvent B was acetonitrile/0.1% TFA, and a linear gradient of 5−40% solvent B over 25 min was used). The fraction containing desired product was collected and lyophilized. The purity and identity of the peptides were determined by analytical HPLC and MALDI-TOF or ESI-MS (Finnigan LTQ), respectively. Gly-Gly-His-COOH (compound **7**) was purchased from Bachem.

UV−vis Absorption Measurements. All UV−vis absorption measurements were carried out using a Cary 100 spectrophotometer using a 1 cm quartz cuvette in 50 mM *N*-ethylmorpholine (NEM) buffer at pH 7.5 unless otherwise specified. The peptides were dissolved in ultrapure water and peptide concentrations were determined by amino acid analysis (Keck Foundation Biotechnology Resource Laboratory, Yale University).

Titrations to Determine Peptide-Metal Binding Stoichiometry. The pH for stoichiometric metal binding studies was determined by measuring the pH dependence of metal binding as judged by UV−vis absorbance. For both cyclic peptide **1** and linear peptide **4**, titrations to determine Cu(II) binding stoichiometry were carried out

dx.doi.org/10.1021/ic302820z | *Inorg. Chem.* 2013, 52, 2729−2735

at pH 7.5. Titrations to determine Ni(II) binding stoichiometry for cyclic peptide **1** and linear peptide **4** were carried out at pH 9.5 and 7.5, respectively. 1.0 mM peptide solution was prepared in 50 mM NEM buffer and baseline was taken to subtract the absorbance of the peptide. 0.1 equiv of metal ion (Cu(II) or Ni(II)) from a freshly prepared 200 mM stock solution was added and the solution was stirred with a magnetic stir bar. UV−vis spectra were recorded in the range of 200 to 900 nm. The solution was equilibrated until there was no change in absorption. This process was repeated until at least 2.0 equiv of metal ion was added. The absorption versus metal:peptide ratio was plotted to determine binding stoichiometries.

pH Dependence of Metal Binding. 1.0 mM peptide was prepared in ultrapure water and baseline was taken to subtract out the absorbance of the peptide. 1.0 equiv of metal ion ($CuCl_2$ or $NiCl_2$) was added to the solution and the pH of the resulting solution was lowered to 2.5, at which no metal binding was observed. Small aliquots (~0.5 μL) of dilute KOH were added to the solution, pH was measured using a microelectrode (3 mm, Mettler Toledo), and absorption spectra were recorded. d−d transition bands centered at ~525 and ~425 nm were observed for Cu(II)-peptide and Ni(II)-peptide complexes, respectively. KOH was added until a saturation point was observed. For plotting pH dependence curves, the absorption was normalized to unity as percent formation of metallopeptide complex and plotted against pH.

EPR Spectroscopy. Fresh Cu-peptide complexes (0.9:1 mM ratio of Cu(II) to peptide in 100 mM Tris-HCl buffer with 10% glycerol) were prepared in capillary tubes and inserted into a quartz EPR tube, then slowly frozen in liquid nitrogen. X-band electron paramagnetic resonance (EPR) data were recorded using a Bruker EMX instrument at a microwave frequency of 9.32 GHz. All spectra were recorded at −150 °C (123 K) using microwave power of 0.64 mW and modulation frequency of 100 kHz. Other instrumental parameters include a sweep width of 1500 G (2250 to 3750 G) for a total of 1024 data points, time constant 655.36 ms, conversion time 163.84 ms, sweep time 167.77 s, and receiver gain 1×10^4 to 2×10^4. All spectra were average of 5 scans. To convert the $A_{\|}$ values (Gauss) into cm^{-1}, the following relation was used:

$$h\nu = g\mu_B . B_o$$

$$hA_{\|} = g_{\|}\mu_B . a_{\|}$$

$$A_{\|} = \left(\frac{\mu_B}{h}\right) g_{\|} . a_{\|} = 1.39 g_{\|} . a_{\|}$$

where A = splitting value in MHz, g = g-value associated with splitting, a = splitting value in Gauss. Then, $A_{\|}$ values in MHz are converted into cm^{-1} using 1 cm^{-1} = 3×10^4 MHz.

Cyclic Voltammetry. A standard three-electrode cell (glassy carbon electrode as working electrode, platinum wire as auxiliary electrode, and saturated calomel electrode (SCE) as a reference electrode) was utilized to perform the electrochemical measurements on a CHI 830 (CH Instrument, Inc., USA). All metallopeptide samples were prepared freshly in water and 100 mM KCl was added as supporting electrolyte. The pH was adjusted as required with KOH/HCl. The sample was purged with nitrogen gas for 5 min before data collection. Scan velocity was 100 mV/s for each scan. Cyclic voltammograms presented are the average of three scans that were then background-subtracted.

DNA Cleavage Assays. 36 μM peptide−metal complexes were prepared using 40 μM peptide and 0.9 equiv $CuCl_2$, in order to ensure copper ion was completely complexed. pUC19 plasmid was used for cleavage experiments as described.[8] While cleavage of supercoiled plasmid DNA does not provide information on site selectivity, it does provide an appropriate initial measurement of broad DNA cleavage activity. Final concentrations of 36 μM Cu(II)-peptide complex, 400 μM ascorbate, 25 μM base-pair concentration of pUC19 plasmid DNA, and 20 mM Tris-HCl Buffer, pH 7.4, were reacted in PCR tubes at 37 °C. At 0.5, 5, 15, 60, and 120 min time points, 25 μL of each reaction was removed and quenched using 5 μL of 0.5 M EDTA solution. 5× formamide-based loading dye was added to each quenched reaction prior to loading in wells of 0.8% agarose gels with ethidium bromide. Gels were run at 100 V for 30 min and UV-imaged using a Bio-Rad Gel-Doc system.

Fluorescence Assay for Detection of Hydroxyl Radicals. 0.9 μM peptide−metal complexes were prepared using 1 μM peptide and 0.9 equiv $CuCl_2$, in order to ensure copper ion was completely complexed. Solutions were prepared using final concentrations of 0.9 μM Cu(II)-peptide complex or $CuCl_2$, 1 mM H_2O_2, 1 mM ascorbate (when applied), 10 μM 2,7-dichlorofluorescein diacetate, in 20 mM HEPES, pH 7.4, and 100 mM NaCl. Total fluorescence intensity was read in 96-well plates using a TECAN infiniTE 200 plate reader with excitation at 485 nm and emission at 535 nm after 60 min incubation at room temperature.

Peptide Binding with Other Metal Ions. Cyclic peptide **1** and linear peptide **4** were incubated with Au(III), Pt(II), or Pd(II) in ultrapure water and the pH was adjusted with dilute HCl to between 2 and 3. Due to the lack of characteristic bands at higher wavelengths for these metal ions, a decrease in UV−vis band of characteristic aqua−metal complexes during the addition of peptide was monitored. Slow changes were observed over the course of hours to days. Following these experiments, the samples were analyzed by ESI-MS spectrometry.

RESULTS AND DISCUSSION

Preparation and Spectroscopic Characterization of Metal−Peptide Complexes. Cyclic peptides **1**−**3** and linear analogues **4**−**6** were synthesized using Fmoc solid-phase synthesis with moderate overall postpurification yields (~20% for cyclic and 60−70% for linear peptides; see Supporting Information for synthesis details). The binding of Cu(II) and Ni(II) to the ATCUN-containing peptides was measured by UV−vis spectroscopy, EPR-spectroscopy, and ESI-MS.

Metal−peptide complexation was found to be highly pH-dependent (Figures 2a,b, S1−2). The absorption spectra of

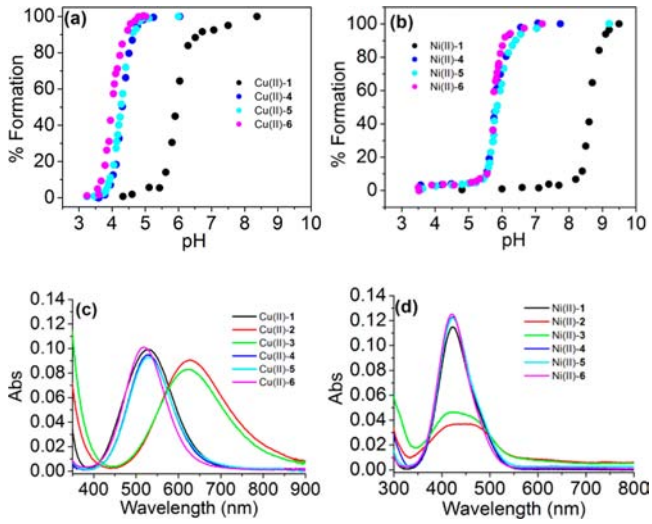

Figure 2. UV−vis spectroscopy of metal-binding peptides. (a) pH dependence of Cu(II) binding to macrocycles and linear analogues. (b) pH dependence of Ni(II) binding to macrocycles and linear analogues. For pH titrations, UV−vis absorbance was monitored as pH was increased with dilute KOH, and normalized absorbance at λ_{max} is plotted against experimentally measured pH. (c) UV−vis spectra of Cu(II)-peptide complexes at pH = 7.5. (d) UV−vis spectra of Ni(II)-peptide complexes at pH = 9.5. All UV−vis spectra were taken using a solution of 1.0 mM metal-peptide complex in 50 mM *N*-ethylmorpholine buffer at 25 °C. Data for metal complexes of peptide **1** are shown in black, **2** in red, **3** in green, **4** in blue, **5** in cyan, and **6** in magenta.

dx.doi.org/10.1021/ic302820z | Inorg. Chem. 2013, 52, 2729−2735

Table 1. Spectroscopic and Electrochemical Data of Metallopeptide Complexes[a]

	Cu(II)-peptide complex						Ni(II)-peptide complex		
	UV−vis		EPR			CV	UV−vis		CV
peptides	λ_{max} (nm)	ε (M^{-1} cm^{-1})	$g_{\|}$	$A_{\|}$ ($\times 10^{-4}$ cm^{-1})	$g_{\|}/A_{\|}$ (cm)	$E_{1/2}$ (mV)	λ_{max} (nm)	ε (M^{-1} cm^{-1})	$E_{1/2}$ (mV)
1	525	99	2.181	202	107.9	739	422	115	irreversible
2	627	90	2.239	193	116.0	–	429	37	–
			2.177*	203	107.2	405*	–	–	–
3	628	83	2.228	194	114.8	–	424	46	–
			2.175*	203	107.1	401*	–	–	–
4	525	95	2.187	200	109.3	802	423	122	730
5	525	94	2.188	200	109.4	809	423	122	–
6	520	100	2.183	202	108.0	740	422	125	–

[a]UV−vis absorptions for Cu(II)-peptide complexes were obtained in 50 mM *N*-ethylmorpholine buffer at pH 7.5. UV−vis absorptions for Ni(II)-peptide complexes were obtained in 50 mM *N*-ethylmorpholine buffer at pH 9.5. EPR was performed in 100 mM Tris-buffer with 10% glycerol at pH 7.5, or at pH 11.5 where indicated (*). Cyclic voltammetry was performed using 1.0 mM peptide-petal complex in 100 mM KCl, at pH 7.5 for Cu-peptide complexes, and at pH 9.5 for Ni-peptide complexes.

Cu(II) mixed with peptides **1**, **4**, **5**, or **6** at pH < 4 showed only a broad, weak band at 800 nm, characteristic of Cu(II) in water. As the pH was slowly raised, the intensity of the d−d transition band at 525 nm increased while the intensity of the 800 nm band decreased. Based on this data, we observed that the linear peptides **4**−**6** each bound Cu(II) with pH transitions between 4 and 4.2, as reported for previous linear ATCUN peptides.[7] Cyclic peptide **1** had an altered pH transition for Cu(II)-binding, with a midpoint near 6.0. Ni(II)-**1** complexation also showed an altered pH transition. Linear peptides **4**−**6** bound Ni(II) with a pH transition near 6.0, in agreement with previously reported values for ATCUN peptides,[7] while the peptide **1**-Ni(II) complex formed with a pH transition nearly three log units higher (midpoint near 8.8). The sharp absorption transitions and lack of variations in λ_{max} at higher pH for peptides **1** and **4**−**6** indicate the formation of single species for each metallopeptide complex.

The altered pH transitions for metal binding observed for cyclic peptide **1** are consistent with previous studies of the macrocycle effect, in which the thermodynamics of complex formation changed when a restrictive macrocycle constraint was applied.[37,38] For Cu(II) binding, linear ATCUN peptides readily form metal complexes by cooperatively deprotonating the imidazolium, ammonium, and amide nitrogens.[2] However, this process appears to be thermodynamically disfavored for cyclic peptide **1**, so that the pH transition of metal binding roughly approximates that of solvent-mediated imidazolium deprotonation. This implies that, in the constrained structure of **1**, the imidazole-Cu(II) coordinate bond is required to position the copper ion for deprotonation of the other nitrogens in order to form the square planar complex. For Ni(II) binding, the pH titrations indicate that the linear ATCUN motifs will form the full complex upon solvent-mediated imidazolium deprotonation. Cyclic peptide **1**, by contrast, appears to require solvent-mediated deprotonation of both the imidazolium and the N-terminal ammonium for complete complexation with Ni(II). We note that this effectively makes cyclic peptide **1** selective for Cu(II) over Ni(II) at physiological pH (Figure S3). While selectivity for Cu(II) over Ni(II) is predicted by the Irving-Williams series, such selectivity has not previously been observed for ATCUN-derived peptides.

UV−vis titration experiments and ESI-MS data demonstrated that the stoichiometry of the metal−peptide complex was 1:1 for cyclic peptide **1** and linear peptide **4** (Figures S4−5). Curve fits to these titrations were unable to produce accurate association constants due to the tight binding affinity, but indicated K_a's of at least 10^8 M^{-1}. The UV−vis absorbance bands observed for Cu(II) complexes of **1**, **4**, **5**, and **6** at pH 7.5 (λ_{max} = 525 nm, ε = 94−100 M^{-1} cm^{-1}) and for Ni(II) complexes of **1**, **4**, **5**, and **6** at pH 9.5 (λ_{max} = 425 nm, ε = 115−125 M^{-1} cm^{-1}) (Table 1), result from d−d transitions consistent with the formation of tetraaza-M(II) complexes in a square planar geometry.[7]

Cyclic peptides **2** and **3** differ from **1** only by the stereochemistry of the macrocycle linker (Figure 1a,b). UV−vis titrations of cyclic peptides **2** and **3** with Cu(II) and Ni(II) produced stepwise transitions indicative of multiple independent deprotonation events (Figure S1−2). In these cases, pH-dependent Cu(II) binding was observed, but the UV−vis and ESI-MS spectra of these complexes are not consistent with square planar, tetraaza-coordination complexes (Figure 2c,d and Figures S1 and S6). The donor ligands at this pH may be the N-terminal amine, the imidazole, and two oxygen atoms from carbonyl groups or water. At pH higher than 10, intensity of the Cu(II)-associated bands for **2** and **3** decrease and an absorption band centered at ∼500 nm starts to appear, maximizing at pH ∼12. Ni(II) binding to **2** and **3** occurs over a broad, two-step transition between pH = 8 and pH = 12, with transition midpoints estimated at roughly 9 and 11 (Figure S2). Altogether, the data on cyclic peptides **2** and **3** indicate that they are capable of forming ATCUN-like metal complexes but only at high pH. Thus, they possess an even greater thermodynamic barrier to complexation than cyclic peptide **1**. This correlates with predictions from the design strategy (Figure 1a), and highlights the critical role of the macrocycle linker in spatial organization of cyclic ATCUN motifs.

EPR Spectroscopy of Copper-Peptide Complexes. Next, EPR spectroscopy was used to further characterize the coordination environment of the Cu(II) center within the Cu(II)-peptide complexes. X-band EPR spectra of Cu(II)-peptide complexes in frozen aqueous solution are shown in Figure 3. All copper-peptide complexes display axial EPR spectra typical for Cu(II) ($g_{\|} > 2.1 > g_{\perp} > 2.00$ and $A_{\|} \approx 158-201 \times 10^{-4}$ cm^{-1}). Specifically, these values are characteristic of the Cu(II) d^9 electron localized in the $d_{x^2-y^2}$ orbital, which indicates a square planar Cu(II) geometry.[39,40] Prior work suggests that the empirical ratio of $g_{\|}/A_{\|}$ correlates with coordination geometry, with the range of 105−120 cm for square planar, 130−150 cm for slight to moderate distortion from square planar, and 180−250 cm for considerable

dx.doi.org/10.1021/ic302820z | Inorg. Chem. 2013, 52, 2729−2735

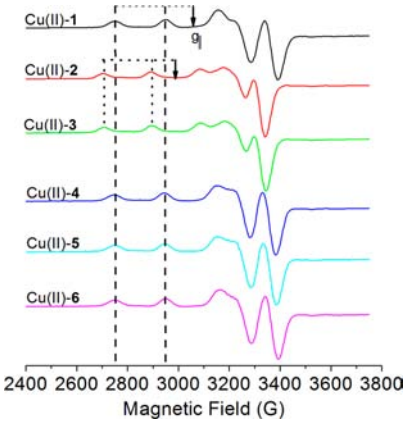

Figure 3. X-band EPR spectra of aqueous Cu(II)-peptide complexes. All spectra were recorded with 1 mM Cu(II)-peptide complex at 123 K in 100 mM Tris-HCl buffer (pH 7.5) and 10% glycerol. The dotted lines highlight the hyperfine splitting due to the coupling of Cu(II) nucleus (I = 3/2) and Cu(II) unpaired electron (s = 1/2). Arrows indicate the $g_{\|}$ associated with the Cu-peptide complexes.

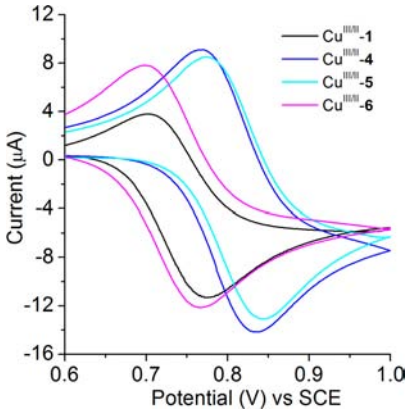

Figure 4. Cyclic voltammetry of copper-peptide complexes. The cyclic votammogram (CV) trace for cyclic peptide **1** is shown in black, with linear analogues **4** in blue, **5** in cyan, and **6** in magenta. The voltammograms were recorded using 1.0 mM peptide-metal complex in 100 mM KCl, pH 7.5, with a scan rate of 100 mV/s.

distortion.[40] For cyclic peptide **1** and linear analogues **4**–**6**, this ratio is roughly 108–109 cm. All these data support a model in which cyclic peptide **1** and linear peptides **4**–**6** each bind Cu(II) in a square planar, tetraaza-coordination sphere at pH 7.5 (Table 1).[41] By contrast, complexes of Cu(II) with cyclic peptides **2** and **3** produced relatively high $g_{\|}$ and low $A_{\|}$ values at pH 7.5 (Table 1). This might suggest a tetrahedral geometry, but if this were the case we would expect to see a higher UV–vis extinction coefficient than that of a square planar tetraaza-complex. Instead, these complexes are likely using a ligand set of two nitrogens and two oxygens for Cu(II) coordination. EPR of Cu(II)-**2** and Cu(II)-**3** at pH 11.5 produced $g_{\|}$ and $A_{\|}$ values close to the values obtained for Cu(II)-**1** at pH = 7.5, indicating the presence of a similar square planar, tetraaza-complex at elevated pH (Figure S7). This supports the conclusion that cyclic peptides **2** and **3** are capable of forming ATCUN-like metal complexes, but cannot do so below pH 11.5.

Cyclic Voltammetry. ATCUN-metal complexes have been shown to allow redox cycling of Cu(III)/Cu(II) and Ni(III)/Ni(II), producing hydroxyl radicals that can be harnessed to cleave and modify biomolecules.[7−19] After observing altered metal-binding properties for cyclic peptide **1**, we asked whether the macrocyclic constraint would alter the redox potential of the metal-peptide complex. The cyclic voltammograms for copper complexes of **1** and **4**–**6** are shown in Figure 4. All four metallopeptides have a quasi-reversible one-electron redox couple for Cu(III)/Cu(II). The Cu(III)/Cu(II)-reduction potential ($E_{1/2}$) for linear analogues **4**, **5**, and **6** are 802, 809, and 740 mV, respectively. The 69 mV difference observed between the $E_{1/2}$ of Cu-**5** and Cu-**6** is attributed to effects of side chain substitutions. This agrees with previous work showing that side chain alterations to nonhistidine residues can similarly affect the redox properties of linear ATCUN peptides.[15,42] Cu-**1** has a reduction potential of 739 mV, essentially identical to the Cu-**6** complex. Thus, for cyclic peptide **1**, macrocyclization is compatible with Cu(III) formation under oxidizing conditions, as has been observed for other cyclic peptides[23] and other macrocycles.[43] Also, the reduction current for the Cu-**1** complex is lower than that of Cu-**4** or Cu-**6** (Figure 4). While still consistent with a quasi-reversible redox process, this finding may indicate an altered Cu(III)-**1** conformation that allows some dissociation of Cu(III) before it can be reduced. Cyclic voltammetry was also performed on nickel complexes of **1** and **4** (Table 1, Figure S8). The Ni-**4** complex displayed a quasi-reversible one-electron redox couple for Ni(III)/Ni(II), with $E_{1/2}$ = 730 mV and ΔE = 100 mV at pH 7.5 consistent with previously reported values for ATCUN motifs.[44] However, irreversible oxidation at 880 mV is observed for the Ni(II)-**1** complex. We speculate that the short-lived Ni(III)-**1** complex rapidly dissociates before it can get reduced to Ni(II), as has been observed for other peptidic Ni(II) ligands.[15,45]

Catalytic Activity of Copper-Peptide Complexes. We next tested the ability of the Cu-**1** complex to oxidatively cleave DNA. Prior work has provided evidence that the ATCUN motif binds DNA in the minor groove, and that side chain substitution can affect DNA binding, rates of Cu(III) formation, and rates of DNA cleavage.[8,15,46] The copper complex of linear peptide **4** showed relatively sluggish DNA cleavage (Figure 5), consistent with previous reports that hydrophobic residues placed C-terminally to the ATCUN motif can impede DNA binding.[47] Linear peptide **7**, which lacks the C-terminal leucine, was used as an additional reference to deconvolute these effects. Cu-**7** cleaves supercoiled plasmid DNA rapidly, with roughly 75% cleavage after 15 min and complete cleavage after 1 h (Figure 5a). These are consistent with reaction rates previously reported for diverse linear ATCUN peptides.[8,9,15] Cu-**1** complexes are able to catalyze oxidative cleavage of DNA even more rapidly, with nearly all the supercoiled DNA cleaved to nicked and linear forms after only 5 min.

To measure catalytic activity more directly, we incubated copper complexes of **1**, **4**, **6**, and **7** with 2,7-dichlorofluorescein diacetate, a profluorescent dye which reacts with hydroxyl radicals (but not peroxides) to form 2,7-dichlorofluorescein in solution.[48] This assay was unable to detect hydroxyl radical formation by all linear ATCUN motifs tested, in accord with previous characterizations.[9] By contrast, Cu-**1** complexes produced hydroxyl radicals in quantities nearly equal to those produced by unliganded Cu(II) ions (Figure 5b), demonstrating the high catalytic activity of this Cu(II) complex. Because linear analogues showed no measurable formation of diffusible radicals, we conclude that the conformational constraint produced by macrocyclization promotes Cu(II)/Cu(III)

dx.doi.org/10.1021/ic302820z | Inorg. Chem. 2013, 52, 2729–2735

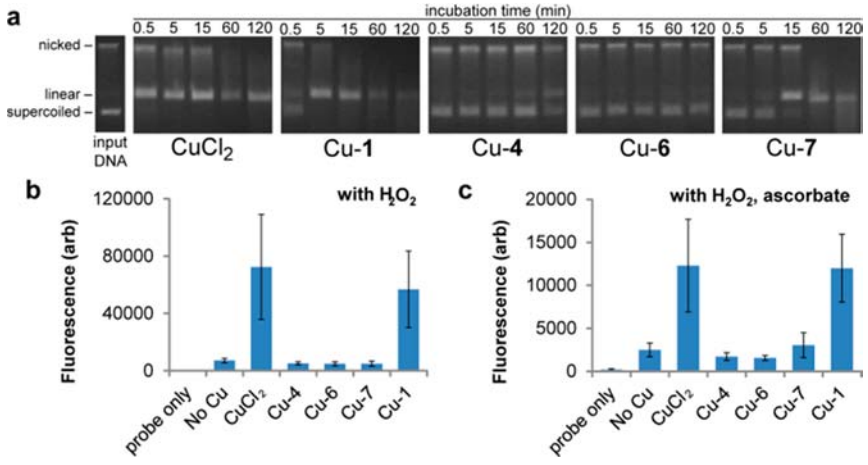

Figure 5. Catalytic activity of copper-peptide complexes. (a) Agarose gels showing cleavage of supercoiled DNA by 36 μM $CuCl_2$ or Cu-peptide complexes. (b) Fluorescence from reaction of diffusible hydroxyl radicals at 25 °C with 10 μM 2,7-dichlorofluorescein diacetate in 20 mM HEPES, pH 7.4, 100 mM NaCl, and 1 mM H_2O_2. "Probe only" trials lacked peroxide. $CuCl_2$ and copper-peptide complexes were tested at 0.9 μM. (c) Experiments identical to (b) were performed in the presence of 1 mM ascorbate. Error bars show standard deviations from 3 independent trials.

cycling relative to linear analogues. Ascorbate is commonly used to promote hydroxyl radical formation and catalytic turnover in copper-redox reactions, so the assay was repeated in the presence of hydrogen peroxide and 1 mM ascorbate.[7−9,15,20,49,50] Under these conditions, we observed lower overall hydroxyl radical generation, but similar enhancement of Cu-**1** redox activity compared to linear analogues (Figure 5c). Peptide integrity during assays with 2,7-dichlorofluorescein diacetate was quantified by LC/MS following 60 min incubation. No degradation of the peptide was observed for the sample treated with peroxide, while some peptide degradation was observed for the sample treated with peroxide and ascorbate. These data indicate that extent of peptide degradation under harsh redox conditions will need to be closely monitored as it is developed as a copper-based oxidation catalyst.

In a recent characterization of diverse Cu(II), Co(II), Ni(II), and Fe(II) complexes, Cowan and co-workers tested nine common copper complexes, and found that all had little or zero radical formation under similar oxidative conditions.[9] Thus, cyclic peptide **1** appears to be unique among a variety of copper ligands in its ability to bind copper without impeding redox cycling between Cu(II) and Cu(III). Structural and spectroscopic analyses investigating this observation are under way.

ATCUN motifs have also been shown to bind other metal cations, including Co(II), Au(III), Pt(II), and Pd(II).[51−53] We incubated **1** and **4** with each of these metal ions and monitored complex formation by UV−vis and ESI-MS. Both peptides bind Au(III), Pt(II), and Pd(II) below a pH of 3.0, with a slow complexation rate ranging from 2 to 3 h for Pd(II) to 1−3 days for Au(III) and Pt(II) (Figure S10−S11). These findings are consistent with literature reports on the complexation of these metal ions with linear ATCUN peptides.[52,54] Linear peptide **4** also rapidly bound Co(II) in a 1:1 complex, as do various other ATCUN peptides previously reported.[9,51,55,56] Cyclic peptide **1**, by contrast, did not bind Co(II) at any pH up to 11.5.

CONCLUSION

In sum, we report a rationally designed, cyclic ATCUN peptide with high affinity for Cu(II) and Ni(II) but altered thermodynamics of metal binding. Cyclic peptide **1** is selective for Cu(II) over Ni(II) and Co(II) at physiological pH, a unique property that could be exploited for sensing applications. The Cu-**1** complex is capable of rapid oxidative cleavage of DNA, and is a powerful catalyst for hydroxyl radical generation. Cu-**1** is distinct from prior cyclic peptide-metal complexes because it tightly binds Cu(II) with minimal hindrance to Cu(III)/Cu(II) redox cycling. Future work exploiting Cu-**1** and related complexes as metallopeptide catalysts will require balancing the production of diffusible oxygen radicals with substrate selectivity to ensure rapid and selective catalysis. In pursuing these complexes as catalysts, we note that they are synthetically accessible and suitable for production of metallopeptide libraries. This will allow rapid testing of variants with different chelate groups and altered macrocycle geometries. This versatility, along with the ability to bind a variety of redox-active metal ions, will facilitate future design of ATCUN macrocycles as chiral, selective catalysts for a variety of chemical transformations.

ASSOCIATED CONTENT

Supporting Information

Characterization data including HPLC, ESI-MS, titration, UV−vis, EPR, CV. This material is available free of charge via the Internet at http://pubs.acs.org.

AUTHOR INFORMATION

Corresponding Author

*Tel.: +1 617-627-0451. Fax: +1 617-627-3443. E-mail address: Joshua.Kritzer@tufts.edu.

Notes

The authors declare no competing financial interest.

ACKNOWLEDGMENTS

We thank Glen O'Neil and Taryn Pallucio for their help in experimental set up of electrochemistry and EPR, respectively. We also thank Dr. Jonathan Bock for MS assistance and Prof. Elena Rybak-Akimova for valuable comments. This work was supported by the National Institutes on Aging of the National Institutes of Health, award number R21AG038776.

REFERENCES

(1) Margerum, D. W. *Pure Appl. Chem.* **1983**, *55*, 23−34.

(2) Sigel, H.; Martin, R. B. *Chem. Rev.* **1982**, *82*, 385−426.
(3) Kozlowski, H.; Bal, W.; Dyba, M.; Kowalik-Jankowska, T. *Coord. Chem. Rev.* **1999**, *184*, 319−346.
(4) Kozlowski, H.; Kowalik-Jankowska, T.; Jezowska-Bojczuk, M. *Coord. Chem. Rev.* **2005**, *249*, 2323−2334.
(5) Sovago, I.; Osz, K. *Dalton Trans.* **2006**, 3841−3854.
(6) Varnagy, K.; Szabo, J.; Sovago, I.; Malandrinos, G.; Hadjiliadis, N.; Sanna, D.; Micera, G. *Dalton Trans.* **2000**, 467−472.
(7) Harford, C.; Sarkar, B. *Acc. Chem. Res.* **1997**, *30*, 123−130.
(8) Jin, Y.; Cowan, J. A. *J. Am. Chem. Soc.* **2005**, *127*, 8408−8415.
(9) Joyner, J. C.; Reichfield, J.; Cowan, J. A. *J. Am. Chem. Soc.* **2011**, *133*, 15613−15626.
(10) Cuenoud, B.; Tarasow, T. M.; Schepartz, A. *Tetrahedron Lett.* **1992**, *33*, 895−898.
(11) Shullenberger, D. F.; Eason, P. D.; Long, E. C. *J. Am. Chem. Soc.* **1993**, *115*, 11038−11039.
(12) Burrows, C. J.; Perez, R. J.; Muller, J. G.; Rokita, S. E. *Pure Appl. Chem.* **1998**, *70*, 275−278.
(13) Liang, Q.; Ananias, D. C.; Long, E. C. *J. Am. Chem. Soc.* **1998**, *120*, 248−257.
(14) Singh, R. K.; Sharma, N. K.; Prasad, R.; Singh, U. P. *Protein Pept. Lett.* **2008**, *15*, 13−19.
(15) Jin, Y.; Lewis, M. A.; Gokhale, N. H.; Long, E. C.; Cowan, J. A. *J. Am. Chem. Soc.* **2007**, *129*, 8353−8361.
(16) Fang, Y. Y.; Ray, B. D.; Claussen, C. A.; Lipkowitz, K. B.; Long, E. C. *J. Am. Chem. Soc.* **2004**, *126*, 5403−5412.
(17) Huang, X. F.; Pieczko, M. E.; Long, E. C. *Biochemistry* **1999**, *38*, 2160−2166.
(18) Horowitz, E. D.; Finn, M. G.; Asokan, A. *ACS Chem. Biol.* **2012**, *7*, 1059−1066.
(19) Gokhale, N. H.; Bradford, S.; Cowan, J. A. *J. Am. Chem. Soc.* **2008**, *130*, 2388−2389.
(20) Kimoto, E.; Tanaka, H.; Gyotoku, J.; Morishige, F.; Pauling, L. *Cancer Res.* **1983**, *43*, 824−828.
(21) Cabbiness, D. K.; Margerum, D. W. *J. Am. Chem. Soc.* **1969**, *91*, 6540−6541.
(22) Hinz, F. P.; Margerum, D. W. *J. Am. Chem. Soc.* **1974**, *96*, 4993−4994.
(23) Rybka, J. S.; Margerum, D. W. *Inorg. Chem.* **1981**, *20*, 1453−1458.
(24) Cram, D. J.; Cram, J. M. *Science* **1974**, *183*, 803−809.
(25) Cram, D. J. *Science* **1988**, *240*, 760−767.
(26) van Veggel, F. C. J. M.; Verboom, W.; Reinhoudt, D. N. *Chem. Rev.* **1994**, *94*, 279−299.
(27) Aime, S.; Batsanov, A. S.; Botta, M.; Dickins, R. S.; Faulkner, S.; Foster, C. E.; Harrison, A.; Howard, J. A. K.; Moloney, J. M.; Norman, T. J.; Parker, D.; Royle, L.; Williams, J. A. G. *Dalton Trans.* **1997**, 3623−3636.
(28) Aime, S.; Botta, M.; Fasano, M.; Terreno, E. *Chem. Soc. Rev.* **1998**, *27*, 19−29.
(29) Galaup, C.; Carrie, M. C.; Azema, J.; Picard, C. *Tetrahedron Lett.* **1998**, *39*, 1573−1576.
(30) Azema, J.; Galaup, C.; Picard, C.; Tisnes, P.; Ramos, P.; Juanes, O.; Rodriguez-Ubis, J. C.; Brunet, E. *Tetrahedron* **2000**, *56*, 2673−2681.
(31) Driggers, E. M.; Hale, S. P.; Lee, J.; Terrett, N. K. *Nat. Rev. Drug Discovery* **2008**, *7*, 608−624.
(32) Baker, B. F.; Lot, S. S.; Kringel, J.; Cheng-Flournoy, S.; Villiet, P.; Sasmor, H. M.; Siwkowski, A. M.; Chappell, L. L.; Morrow, J. R. *Nucleic Acids Res.* **1999**, *27*, 1547−1551.
(33) Brasun, J.; Gabbiani, C.; Ginanneschi, M.; Messori, L.; Orfei, M.; Swiatek-Kozlowska, J. *J. Inorg. Biochem.* **2004**, *98*, 2016−2021.
(34) Brasun, J.; Matera, A.; Oldziej, S.; Swiatek-Kozlowska, J.; Messori, L.; Gabbiani, C.; Orfei, M.; Ginanneschi, M. *J. Inorg. Biochem.* **2007**, *101*, 452−460.
(35) Camerman, N.; Camerman, A.; Sarkar, B. *Can. J. Chem.* **1976**, *54*, 1309−1316.
(36) Chan, W. C.; White, P. D. *Fmoc Solid-Phase Peptide Synthesis: A Practical Approach*; Oxford University Press: New York, 2000.
(37) Lin, C.-T.; Rorabacher, D. B.; Cayley, G. R.; Margerum, D. W. *Inorg. Chem.* **1975**, *14*, 919−925.
(38) Izatt, R. M.; Bradshaw, J. S.; Nielsen, S. A.; Lamb, J. D.; Christensen, J. J. *Chem. Rev.* **1985**, *85*, 271−339.
(39) Lucchese, B.; Humphreys, K. J.; Lee, D.-H.; Incarvito, C. D.; Sommer, R. D.; Rheingold, A. L.; Karlin, K. D. *Inorg. Chem.* **2004**, *43*, 5987−5998.
(40) Addison, A. W., Spectroscopic and redox trends from model copper complexes, in *Copper Coordination Chemistry: Biochemical and Inorganic Perspectives*, Karlin, K. D.; Zubieta, J., Eds.; Adenine Press: New York, 1983.
(41) Peisach, J.; Blumberg, W. E. *Arch. Biochem. Biophys.* **1974**, *165*, 691−708.
(42) Laussac, J. P.; Sarker, B. *Biochemistry* **1984**, *23*, 2832−2838.
(43) Hanss, J.; Beckmann, A.; Kruger, H.-J. *Eur. J. Inorg. Chem.* **1999**, 163−172.
(44) Bossu, F. P.; Margerum, D. W. *Inorg. Chem.* **1977**, *16*, 1210−1214.
(45) Tesfai, T. M.; Green, B. J.; Margerum, D. W. *Inorg. Chem.* **2004**, *43*, 6726−6733.
(46) Wilson, D. P.; Wan, Z.-K.; Xu, W.-X.; Kirincich, S. J.; Follows, B. C.; Joseph-McCarthy, D.; Foreman, K.; Moretto, A.; Wu, J.; Zhu, M.; Binnun, E.; Zhang, Y.-L.; Tam, M.; Erbe, D. V.; Tobin, J.; Xu, X.; Leung, L.; Shilling, A.; Tam, S. Y.; Mansour, T. S.; Lee, J. *J. Med. Chem.* **2007**, *50*, 4681−4698.
(47) Nagane, R.; Koshigoe, T.; Chikira, M. *J. Inorg. Biochem.* **2003**, *93*, 204−212.
(48) Myhre, O.; Andersen, J. M.; Aarnes, H.; Fonnum, F. *Biochem. Pharmacol.* **2003**, *65*, 1575−1582.
(49) Pamatong, F. V.; Detmer, C. A.; Bocarsly, J. R. *J. Am. Chem. Soc.* **1996**, *118*, 5339−5345.
(50) Detmer, C. A.; Pamatong, F. V.; Bocarsly, J. R. *Inorg. Chem.* **1996**, *35*, 6292−6298.
(51) Ananias, D. C.; Long, E. C. *J. Am. Chem. Soc.* **2000**, *122*, 10460−10461.
(52) Best, S. L.; Chattopadhyay, T. K.; Djuran, M. I.; Palmer, R. A.; Sadler, P. J.; Sovago, I.; Varnagy, K. *Dalton Trans.* **1997**, 2587−2596.
(53) Kirvan, G. E.; Margerum, D. W. *Inorg. Chem.* **1985**, *24*, 3017−3021.
(54) Glisic, B. D.; Rajkovic, S.; Zivkovic, M. D.; Djuran, M. I. *Bioorg. Chem.* **2010**, *38*, 144−148.
(55) Lakusta, H.; Sarkar, B. *J. Inorg. Biochem.* **1979**, *11*, 303−315.
(56) Hawkins, C. J.; Martin, J. *Inorg. Chem.* **1983**, *22*, 3879−3883.